Clim. Past Discuss., 9, 1565–1597, 2013
www.clim-past-discuss.net/9/1565/2013/
doi:10.5194/cpd-9-1565-2013

Climate of the Past Discussions
Open Access

LGM permafrost distribution: how well can the latest PMIP multi-model ensembles reconstruct?

K. Saito[1,2], T. Sueyoshi[2], S. Marchenko[3], V. Romanovsky[3,4], B. Otto-Bliesner[5], J. Walsh[1], N. Bigelow[6], A. Hendricks[1], and K. Yoshikawa[7]

[1]International Arctic Research Center, University of Alaska Fairbanks, Fairbanks, USA
[2]Japan Agency for Marine-Earth Science and Technology, Yokohama, Japan
[3]Geophysical Institute, University of Alaska Fairbanks, Fairbanks, USA
[4]Earth Cryosphere Institute, Tyumen, Russia
[5]National Center for Atmospheric Research, Boulder, USA
[6]Alaska Quaternary Center, University of Alaska Fairbanks, Fairbanks, USA
[7]Water and Environmental Research Center, University of Alaska Fairbanks, Fairbanks, USA

Received: 27 February 2013 – Accepted: 11 March 2013 – Published: 25 March 2013

Correspondence to: K. Saito (ksaito@iarc.uaf.edu)

Published by Copernicus Publications on behalf of the European Geosciences Union.

Abstract

Global-scale frozen ground distribution during the Last Glacial Maximum (LGM) was reconstructed using multi-model ensembles of global climate models, and then compared with evidence-based knowledge and earlier numerical results. Modeled soil temperatures, taken from Paleoclimate Modelling Intercomparison Project Phase III (PMIP3) simulations, were used to diagnose the subsurface thermal regime and determine underlying frozen ground types for the present-day (pre-industrial; 0 k) and the LGM (21 k). This direct method was then compared to the earlier indirect method, which categorizes the underlying frozen ground type from surface air temperature, applied to both the PMIP2 (phase II) and PMIP3 products. Both direct and indirect diagnoses for 0 k showed strong agreement with the present-day observation-based map, although the soil temperature ensemble showed a higher diversity among the models partly due to varying complexity of the implemented subsurface processes. The area of continuous permafrost estimated by the multi-model analysis was 25.6 million km^2 for LGM, in contrast to 12.7 million km^2 for the pre-industrial control, whereas seasonally, frozen ground increased from 22.5 million km^2 to 32.6 million km^2. These changes in area resulted mainly from a cooler climate at LGM, but other factors as well, such as the presence of huge land ice sheets and the consequent expansion of total land area due to sea-level change. LGM permafrost boundaries modeled by the PMIP3 ensemble-improved over those of the PMIP2 due to higher spatial resolutions and improved climatology-also compared better to previous knowledge derived from the geomorphological and geocryological evidences. Combinatorial applications of coupled climate models and detailed stand-alone physical-ecological models for the cold-region terrestrial, paleo-, and modern climates will advance our understanding of the functionality and variability of the frozen ground subsystem in the global eco-climate system.

CPD
9, 1565–1597, 2013

1 Introduction

Frozen ground (permafrost and seasonally frozen ground) constitutes a critical environmental subsystem of the Arctic eco-climate, closely linked with snow and vegetation (Nelson, 2003; Saito et al., 2013). It can affect local and remote regions through interactions and feedbacks between energy, momentum, water, and materials (carbon, nitrogen, etc.). This subsystem has shown an enhanced and wide response to the recent global warming trend (Romanovsky et al., 2010a, b; Smith et al., 2010; Christiansen et al., 2010). Understanding its functionality, variations, and stability under a different (e.g., glacial) and/or changing (e.g., the present-day) climate is a crucial element in Earth science research, as well as in social sciences and policy-making (UNEP, 2012). The areal extent of permafrost during the Last Glacial Maximum (LGM) has been mapped using regional to local evidence (e.g., Baulin and Danilova, 1984; Velichko et al., 1984; Franzel et al., 1992; Baulin et al., 1992; Petit-Maire et al., 2000; French, 2007); the northern and western parts of Eurasia and the northern parts of North America and Greenland have been defined relatively well (Vandenberghe et al., 2008; Hubberten et al., 2004; Rozenbaum and Shpolyanskaya, 1998; Washburn, 1980), especially when compared with other areas such as Northeast Asia (Vandenberghe et al., 2004, 2012; Saito, 2012; Saito et al., 2013) and the Southern Hemisphere (Trombotto et al., 2008; Saito, 2012).

Numerical reconstructions of subsurface temperature regimes from past glacial periods to the present day have been investigated in Alaska, Europe, and Siberia, with comparison to borehole temperature or permafrost thickness data (Lachenbruch et al., 1982; Osterkamp and Gosink, 1991; Delisle, 1998; Delisle et al., 2004; Sueyoshi and Hamano, 2004; Kitover et al., 2012). While these analyses provided minute information about permafrost evolution at sites under climatic changes, they are not easily extended to wider areas such as continents or hemispheres, partly owing to scarce networks of deep borehole data and to high heterogeneity of the terrain.

CPD
9, 1565–1597, 2013

Large-scale climate models, from generations of General Circulation Models to advanced Global Climate Models (hereafter, GCMs) and Earth System Models (ESMs), have been used for global-scale paleoclimate studies since the 1970s (Gates, 1976). However, less attention has been paid to the terrestrial dynamics, including those at high latitude regions, until recently. At the time of the Paleoclimate Modelling Intercomparison Project phase II (PMIP2; Braconnot et al., 2007), subsurface variables such as soil temperature and soil moisture were not archived within the common database. It was in the 2000s that the subsurface regime modelled by GCMs began to undergo intensive analysis (Lawrence and Slater, 2005; Saito et al., 2007). Subsequently, the shortcomings and problems of the processes implemented in the earlier-generation GCMs have been widely addressed and improved (e.g., Nicholsky et al., 2007; Alexeev et al., 2007; Saito, 2008; Lawrence and Slater, 2010). In the third phase of PMIP (PMIP3 2011), conducted in tandem with the fifth phase of the Climate Modelling Intercomparison Project (CMIP5; Talor et al., 2012), a number of subsurface variables (for soil columns ranging from 3 m to 44 m in depth) are archived in the common database, made publicly available, and used for analysis (e.g., Koven et al., 2013).

When and where subsurface temperature is not available, mean annual surface air temperature (MAAT) is a surrogate variable commonly used to interpret and distinguish types of underlying permafrost (Washburn, 1980; French, 2007; Matsuoka, 2011; Gruber et al., 2012; Boeckl et al., 2012). Van Vliet-Lanoë (2009) provides the rough criteria: MAAT $< -7\,^{\circ}$C for permafrost zones covering more than 80 % of the area, $-7\,^{\circ}$C $<$ MAAT $< -3\,^{\circ}$C for zones with permafrost coverage less than 80 %, and $-3\,^{\circ}$C $<$ MAAT for patchy permafrost. However, threshold values are different for different application areas, periods, and types of permafrost (for example, Washburn, 1980, cites $-2\,^{\circ}$C as the upward limit for permafrost, and uases the range of $-5\,^{\circ}$C to $-10\,^{\circ}$C for the presence of continuous permafrost for different regions). This is partly a manifestation that subsurface thermal regime is not a function of air temperature alone, but depends also on other factors such as snow cover, vegetation, soils, and microtopography (Saito et al., 2013). Still dependent on atmospheric thermal information

CPD
9, 1565–1597, 2013

alone, however, the use of freeze and thaw indices (defined as cumulative degree-days below and above 0 °C, respectively) have been attempted to improve the classification of frozen ground types (Harris, 1981, 1982; Anisimov and Nelson, 1997; Saito et al., 2009).

Saito et al. (2009) utilized the PMIP2 surface air temperature outputs to derive freeze and thaw indices, in order to estimate frozen ground distribution at 0 k and LGM, and assessed these estimations using the evidence-based maps. Partly due to coarseness of the horizontal resolution, these comparisons produced mixed results consistent with evidence in some regions but not in others, including north of the Alps, high mountainous regions such as the Tibetan Plateau in the Northern Hemisphere, and the Andes and Tierra del Fuego in the Southern Hemisphere. These discrepancies, however, also resulted from known biases in PMIP2 products (e.g., warm bias in the Western Europe winter; Ramstein et al., 2007; Braconnot et al., 2007). Upon simulation outputs of the PMIP3 experiments becoming publicly available, this is a perfect time for assessing the models' ability to reconstruct LGM frozen ground, as there is an effort from the observational side for an Action Group of the International Permafrost Association (IPA) – "Permafrost Extension during the Last Permafrost Maximum (LPM) in the Northern Hemisphere" – to compile and publish in 2013 an evidence-based map of maximum permafrost extent during the last glaciations period (J. Vandenberghe and H. French, personal communication, 2013).

The issues this study attempts to address are:

- How good are explicitly computed cold-region near-surface ground states in the PMIP3 models that employ newer generation GCMs/ESMs, with improved physics and finer spatial resolutions? And how do the modeled ground temperature distributions compare with previous knowledge from the evidence-based maps?

- How is the information regarding modeled surface and subsurface temperatures on a grid box associated with and consolidated into the frozen-ground zonation in the area represented by the grid?

CPD
9, 1565–1597, 2013

– How well do the derived distributions reconstruct permafrost boundary locations (especially in the Northern Hemisphere)?

This paper provides a descriptive analysis about the multi-model PMIP3 ensemble, with respect to distribution of modeled surface and subsurface thermal states, and geographical extent of reconstructed near-surface frozen ground. Progress in modeling frozen ground characteristics post-PMIP2 simulations is assessed by comparisons with the evidence-based knowledge and maps currently available.

2 Methodology

2.1 Experimental design and boundary conditions

Simulations by global paleoclimate models that participated to PMIP2 (Braconnot et al., 2007) and PMIP3 (PMIP3 2012) were used in this study for the pre-industrial (piControl; 0 k) and the Last Glacial Maximum (LGM; 21 k) periods. Summary of the used models, institutes or groups, and simulations is summarized in Table 1.

In PMIP3 simulations, orbital parameters (e.g., eccentricity and obliquity) and trace gas concentrations (such as carbon dioxide, methane, N_2O, CFC, and ozone) were prescribed to the common values for the respective period of 0 k and 21 k (cf. PMIP3 https://wiki.lsce.ipsl.fr/pmip3/doku.php/pmip3:design:21k:final for 21 k, and https://wiki.lsce.ipsl.fr/pmip3/doku.php/pmip3:design:pi:final for 0 k). The pre-industrial control run experiment of PMIP3 is common to and follows the design specification and boundary conditions determined by the CMIP5 experiment protocol (consult Taylor et al., 2012, for details). Ice-sheet extent and land/sea distribution, and also their altitude (topography) at the LGM period were also prescribed commonly by the participating models. The used ice sheet extent was a blend product of ICE-6G v2.0 (Peltier et al., 2010), MOCA (Tarasov and Peltier, 2002, 2003), and ANU (Lambeck et al., 2004). The detailed information is available at PMIP3 https://wiki.lsce.ipsl.fr/pmip3/doku.php/pmip3:design:pi:final:icesheet. Vegetation was either computed by the model or prescribed

CPD
9, 1565–1597, 2013

to the pre-industrial conditions. We did not stratify the analysis by the difference of vegetation distribution or mechanisms in this study, which is left for future research.

In PMIP2 experiments, the binding of the use of common boundary conditions were not strict, and, therefore, the orography, land/sea mask, and extent and height of ice sheets were various among the models. Braconnot et al. (2007) describe a detail of the specifications of the participating models.

All the boundary conditions and monthly temperature data in PMIP2 and PMIP3 were provided in a netCDF format. The PMIP3 data files were taken from the Earth System Grid Federation (ESGF) system, common to the other CMIP5 data (for example, at http://pcmdi9.llnl.gov/esgf-web-fe/). The PMIP2 data files were taken from the PMIP2 database at http://pmip2.lsce.ipsl.fr/database. The climatology of the variables, i.e., surface air and subsurface temperatures, was computed using the last ten years of the simulations.

Since the horizontal resolutions (i.e., number of grid boxes in the longitude and latitude directions) are different from one model to another (Table 1), spatial interpolation was performed in advance of analysis to a respective common grid system for PMIP2 and PMIP3 by choosing the finest resolution among the models used in the analysis. For PMIP2 it was 128 grids in longitude and 64 grids in latitude (approximately 2.8 degrees by 2.8 degrees resolution), while it was 288 by 192 grid boxes (approximately, 1.25 degrees by 0.94 degrees) for PMIP3. A common mask for PMIP2 ice sheet and ocean for analysis and display were determined in each grid box by a majority principle among the models used.

2.2 Frozen ground zonation

Permafrost is defined as “ground (soil or rock and included ice and organic material) that remains at or below 0 °C for at least two consecutive years” by the International Permafrost Association (IPA; van Everdingen, 1998). According to this definition, permafrost regions can be divided into *continuous* and *discontinuous* permafrost zones – in the former, “permafrost occurs everywhere beneath the exposed land surface”,

CPD
9, 1565–1597, 2013

or practically more than 90 % of the area underlain by permafrost, while in the latter "permafrost occurs in some areas beneath the exposed land surface throughout a geographic region where other areas are free of permafrost". In the "Circum-arctic map of permafrost and ground-ice conditions" (the IPA map; Brown et al., 1998), however, a part of a discontinuous permafrost zone is further subdivided to *sporadic* and *isolated* permafrost zones, in which 10–50 % and 0–10 % of the area is underlain by permafrost, respectively. In this study, frozen ground zones were classified into the following five categories: "continuous permafrost", "discontinuous permafrost", "sporadic/isolated permafrost", "seasonally frozen ground" (that freezes and thaws annually), and "no freezing".

In a grid box, soil temperature output (T_{sl}) can determine explicitly the frozen ground type in terms of permafrost, seasonally frozen ground, or no freezing. For example, if temperature remains at or below 0 °C at any soil layer for two consecutive years or longer, it is permafrost. If the top soil layers freeze and thaw annually, however, it is seasonally frozen. And if the temperature remains above 0 °C, it is not freezing. However, frozen ground distribution is an areal zonation of the subsurface thermal regime, and it is not trivial to determine from the GCM output for grid boxes that represent areas on a scale order of 1° square (approximately 10 000 km^2) or larger, as shown in the analysis. In this study, frozen ground zones from monthly soil temperature were determined by the following criteria (T_{sl}-based criteria):

"Continuous": the bottom soil layer is frozen (at or below 0°C) for the entire period.

"Discontinuous": the bottom soil layer is frozen for more than half of the period.

"Seasonal": the top soil layer is frozen for more than 30 % of the period.

"Intermittent": only episodic freezing occurs at the top soil layer.

"No freezing": no freezing occurs at any layer. (1)

Since no soil temperature was archived in the PMIP2 database, it was not possible to compute the subsurface thermal regime directly. Saito et al. (2009) developed an indirect methodology for using air temperature at the surface (T_{as}) to estimate the frozen

CPD
9, 1565–1597, 2013

ground type underneath. They employed freeze and thaw indices – originally based on daily values, but computed from the modeled monthly mean outputs (Saito et al., 2009; Frauenfeld et al., 2007). By comparing the 0.5°-grid IPA map (Brown et al., 1998) and the 1981–2000 climatology of the Equal-Area 25 km-grid freeze index (I_f) and thaw index (I_t) interpolated and compiled by Zhang et al. (2007) from the 0.5 × 0.5-degree Climate Research Unit (CRU) data (Mitchell and Jones, 2005), T_{as}-based criteria was constructed as:

$$\begin{aligned}
&\mathrm{Pf}: I_t < 0.8I_f - 1800\\
&\mathrm{Tr}: 0.8I_f - 1800 < I_t < 0.8I_f - 680\\
&\mathrm{Sf}: 0.8I_f - 680 < I_t \quad \text{and} \quad \mathrm{MAAT} < 0\\
&\mathrm{Im}: \mathrm{MAAT} >= 0 \quad \text{and} \quad I_f > 0\\
&\mathrm{Nf}: I_f = 0
\end{aligned} \tag{2}$$

Here, MAAT is mean annual surface air temperature. A comparison of the T_{as}-based map produced from the observed freeze and thaw indices with the present-day IPA map resulted in category correspondence in the following manner: Pf to "continuous permafrost", Tr to "discontinuous permafrost", Sf to "sporadic to isolated permafrost", Im to "seasonally frozen ground", and Nf to "no freezing" (Saito et al., 2009, 2013).

In the analyses in this study, the statistics are shown by the multi-model median (50th percentile value) rather than arithmetic mean because the number of samples used in the analysis was not large enough to evaluate the Gaussian assumption.

3 Simulated surface temperature climatology

Climatological differences in the atmospheric thermal conditions at the surface for the LGM, relative to the pre-industrial period, were evaluated for PMIP2 and PMIP3 (Fig. 1). Freeze indices measure the severity of the cold season, while thaw indices denote warm season characteristics. An increase in freezing index in the middle to high

CPD
9, 1565–1597, 2013

latitudes was commonly found in the PMIP3 and PMIP2 in the Northern Hemisphere. This increase was enhanced for the PMIP3, reaching up to 7000 °C-days along the southern boundary of the continental ice sheets (for the Laurentide and Fennoscandian ice sheets, especially), and up to 4000 °C-days in the northern areas across Eurasia and North America, including Beringia (Fig. 1a and b). This increase means either additional cooling during the sub-zero season or extension of the season, or both. Also noted was the cooling in the mountain ranges from Caucasus to the Pamir, the Tibetan and Ordus Plateau, by up to 2500 °C-days along the southern limit of the freezing zones. In the Southern Hemisphere, the highest part of the Andes showed a similar cooling at a magnitude of up to 2000 °C-days. An overall decrease in global thaw index is found in both the experiments, except for some warming in northeast Eurasia (Fig. 1c and d). Similar to the increase in the freeze index, this trend indicates either a decrease in the warm season temperature or a shortening of the season, or both. These results are in line.

MAAT is an amalgamation of the two indices (i.e., MAAT = $(I_t - I_f)/365$). The maps of MAAT show clearly that the overall characteristics in MAAT difference are governed by the cold season trend both in PMIP2 and PMIP3 (Fig. 1e and f). One important implication is that the degrees of cooling at 21 k between the cold and warm seasons (i.e., changes in I_f and I_t) were different from region to region. The geographical distribution of this difference in the seasonality, or asymmetry, is essential to interpreting the spatial difference of frozen ground response, resulting in the sometimes not enough or misleading use of MAAT (Harris, 1981, 1982). Previous experiences indicated that this is especially applicable in the cases of "coarse" spatial scales of 10 000 km^2 or larger, where the effects of other small-scale factors are apt to be smoothed out by spatial averaging (Saito et al., 2009, 2013).

CPD
9, 1565–1597, 2013

4 Modeled distributions of frozen ground and its inter-model diversity

4.1 Present-day frozen ground distributions

The frozen ground distributions reconstructed by the direct method using soil temperature (T_{sl}-criteria) and the indirect method using surface air temperature (T_{as}-criteria) are shown in Fig. 2, together with the observation-based map. The 0 k reconstructions from the PMIP3 products (Fig. 2a and c) compare well in general to observations (Fig. 2g), both in Eurasia and North America. The PMIP2 product (Fig. 2e) is also consistent with observations but failed to represent regional details due to coarse resolution, especially in the areas with complex relief – e.g., the Altai and Rocky mountains. Presence of permafrost at the Tibetan Plateau was reproduced in all cases, which is sometimes difficult because of smoothed orography in the models (leading to underestimation of temperatures).

The T_{sl}-based map (Fig. 2a) showed large dark green areas, which are defined by freezing of the top soil layer for more than 30 % of the period (about 4 months or longer) but no continuing freezing at the bottom of the soil column, and named as a "Sporadic/Isolated" zone. Compared to the T_{as}-based estimate (i.e., "Sf" zones), these areas are overestimated. According to historical soil temperature data from the former Soviet Union, these areas are seasonally frozen ground regions (Fig. 1 of Frauenfeld et al., 2004). This is one example of the gap between a point soil temperature profile and the determination of an areal zonation. These discrepancies from the observations may also have resulted from the time difference between the pre-industrial period (assuming years around 1850; Taylor et al., 2012) and observations for the IPA map (late 20th century). This is likely, thanks to recovery from the Little Ice Age and a long time constant of frozen ground dynamics. In fact, Koven et al. (2013) showed that the modeled permafrost area for 1850 changed by 2005 by a value ranging from 2 % (increase) to −47 % (decrease) in the CMIP5 multi-model simulations. Another factor, not irrelevant to the previous point, is that the piControl experiment is an equilibrium experiment, while the IPA map includes transient states of the permafrost system. The T_{as}-based

CPD
9, 1565–1597, 2013

method, however, reproduced a result closer to the IPA map. Considering the shorter time scale of atmospheric temperature relative to its subsurface counterpart, the discrepancies between the T_{sl}-based map and observations is rather due to the issue of associating point value to a zone of areal extent, and/or implemented subsurface physics.

The finer resolution of PMIP3 definitely contributed to the improvement of T_{as}-based maps from PMIP2. PIMIP3 is less zonal and shows the orography effects clearly. One of the advantages of T_{as}-based methodology is its flexibility to downscale. With use of fine-resolution digital elevation models (DEMs) and assumed lapse rate of temperature with height, surface air temperature data from the GCM outputs or observation-derived maps (for example, reanalysis data) can be used to produce a downscaled frozen ground distribution map. This application has been conducted for Northeast Asia (Saito et al., 2013), Japan (Saito et al., 2012), and South America (Saito et al., 2012). See also discussions in Sect. 5.

4.2 LGM permafrost distribution

The LGM permafrost maps reconstructed from observational evidence in the previous studies shows equatorward expansion of permafrost and seasonally frozen ground regions due to cooler and drier climates at the time. Permafrost in Eurasia covered areas between the Fennoscandian ice sheet and the Alps, the northern Dnieper and Volga river basins, Western and Central Siberia, the Altai and Mongolian highlands, and Northern Asia (Baulin and Danilova, 1984; Velichko et al., 1984; Baulin et al., 1992; Frenzel et al., 1992; Vandenberghe and Pissart, 1993; Xu et al., 1988; Ono 1990, 1991; Petit-Maire et al., 2000; Vandenberghe et al., 2004; French, 2007). In North America, continuous permafrost occupied up to 40° N and south even to the middle of the continent, with a 2–8° wide latitudinal band of discontinuous permafrost zone to its south (French, 2007).

The frozen ground maps from the PMIP products were in good correspondence to each other (Fig. 2b, d, and f). Obvious improvement from the PMIP2 products included

CPD
9, 1565–1597, 2013

the presence of permafrost to the north of the Alps (Fig. 2b and d). The more zonally symmetric feature of the LGM permafrost boundary that Velichko and Nachaev (1984) suggested was also successfully reproduced in the PMIP3 products.

Differences among the methods are more apparent near the borders between seasonal and non freezing zones, and in the Southern Hemisphere. However, there is not enough evidence to validate the boundaries between the seasonal and non freezing zones, even for the present day. For the Southern Hemisphere, geomorphological evidence was reported for mountain permafrost in the Andes and Tierra del Fuego during the Last Glacial period (Trombotto, 2002). The T_{sl}-based estimate produced areas with presence of LGM permafrost more clearly than the T_{as}-based did, and appeared closer to the field observations. The PMIP2 product was in general too coarse for mountain permafrost reconstruction; despite some hint of permafrost presence reproduced at the highest area of the Andes.

The statistics on the areal extent of frozen ground regions at 21 k and 0 k and their changes are summarized in Table 2. The IPA map reports about 11.0 and 4.3 million km^2 areas of continuous and discontinuous permafrost, respectively (Brown et al., 1998). The multi-model results for 0 k are within this range (see also Table 2 of Koven et al., 2013), although the T_{sl}-based median is apparently an underestimate. Continuous permafrost increased at 21 k relative to 0 k in all cases, though the differences varied among the experiments and methods from 2 to 13 million km^2, partly due to coarse horizontal resolution. Despite an increase in land area by coast line advance, the net area increase was not large, due to occupation by the large ice sheets (especially in North America and Scandinavia). The change in areal extent of discontinuous permafrost was controversial among the methods. A slight increase of 0.4 million km^2 at LGM was estimated by the T_{sl}-based method, while the T_{as}-based method estimated decreases by about 2 million km^2 for both experiments. Seasonally frozen ground showed unanimous decrease for the LGM, with values of about 10 million km^2 – almost equal among the methods. These decreases owed mainly to the little changes in winter temperatures in the equatorial regions between the period (Fig. 1a) so that the southern boundaries (in

CPD
9, 1565–1597, 2013

the Northern Hemisphere) of the seasonal frozen ground zone did not expand, relative to the equatorward at 21 k.

4.3 Inter-model diversity

Figure 3 shows the variations, or diversity, of the estimated frozen ground types among the models for each method, measured by the quantity $H = -\Sigma p_i \ln(p_i)$, known as the Shannon-Wiener index, defined by the classification probability p_i, for the ith category (Shannon, 1948). Areas of high diversity (shown in reddish colors) denote regions of dispute among the models, while zero diversity means that the resulting type is unanimous. The T_{sl}-based classification showed higher diversity, in general, than the T_{as}-based one for 0 k (Fig. 3a and c). The areas of high diversity shifted southward for the 21 k, and the values of diversity were largely greater, reflecting a cooling tendency and general diversity of the modeled climate among the models.

High diversity appears along the boundaries between adjacent frozen ground types (e.g., continuous and discontinuous, permafrost and seasonal). The high diversity areas of the T_{as}-based maps are concentrated on the boundaries between permafrost and seasonally frozen ground, while such areas tend to spread wider in the case of the T_{sl}-based map. These results imply larger differences between simulated subsurface thermal regimes among the models, which may be due to differences in implemented physics regarding freeze-thaw processes among the models. The high diversity found in the PMIP2 0 k map owes partly to differences in boundary conditions among the models, such as ice sheets, land/sea mask and orography distribution (Fig. 3e).

5 Modeled subsurface thermal regime

Seasonal change in the top soil layer in the frozen ground zone is a direct concern to the eco-climate system, and, in modern times, to the anthroposphere (including the socio-economy) as well. It is in the active layer (seasonally thawed layer) in the permafrost

CPD
9, 1565–1597, 2013

zones that the most of the hydrological and biogeochemical activities take place. Its thickness defines the volume in which water is hold and drained and the realm in which the root systems can grow and other biotic matters take up nutrients. In the seasonally frozen ground zone, the length and depth of the frozen layer restrict the surface infiltration and biotic activities including agriculture. The seasonality of the subsurface thermal regime is closely related to the phenology in the regions. The thickness of active layer is a measure of changes in permafrost (i.e., aggradation and degradation). The multi-model median of maximum active layer thickness (ALT) is known to have close connection to summertime temperature while maximum seasonal freezing depth (SFD) is related to winter temperate (and snow depth). Figure 4 shows ALT (in red) in permafrost regions, and SFD (in blue) in seasonally frozen ground regions, computed from the monthly soil temperature profiles. Table 3 summarizes the areal extent of different ALT and SFD for the two periods. The results show shallower active layer and deeper seasonal freezing for the LGM, which is consistent with the changes in freeze and thaw indices (Fig. 1).

The LGM southern boundaries of latitudinal permafrost zone (i.e., excluding the altitudinal/mountain permafrost such as the Tibetan Plateau) reconstructed from the observational evidences are around 48–50° N for Asia, 47–49° N for Asian Russia to east Europe, 44–47° N and north of the Alps in west Europe in Eurasia (Baulin and Danilova, 1984; Velichko et al., 1984; Baulin et al., 1992; Frenzel et al., 1992; Vandenberghe and Pissart, 1993; Petit-Maire et al., 2000; Vandenberghe et al., 2004; French, 2007). Xu et al. (1988) and Ono (1990, 1991) argues that the southern boundary of permafrost advanced to the 40° N latitude in Northeast Asia. French (2007) suggested the southern boundary of continuous permafrost advanced also up to 40° N to the south of the Laurentide ice sheet in the North America.

Figure 5a and b extracted the boundaries for continuous and discontinuous permafrost, respectively, taken from Fig. 2. The present-day boundaries taken from the observation (the IPA map) are shown in red. The modeled boundaries for the LGM (thick lines) are in general in good correspondence to the evidence-based knowledge

CPD
9, 1565–1597, 2013

described above. The more "latitudinal" feature (i.e., parallel to the latitude lines) for the LGM than for the present-day is clearly seen, as indicated by Velichko and Nachaev (1984).

The first implication of these figures is that the discontinuous permafrost boundary agrees better among the three lines than does the continuous permafrost boundary, in both Eurasia and North America, and for 0 k and 21 k. The *Tr*-"discontinuous"-boundary appeals to be a robust criterion. Secondly, the direct (T_{sl}-base) method does not necessarily produce a better estimate, as the indirect (T_{as}-based) method shows a closer correspondence with the observations (e.g., in eastern Siberia and northern Canada, for the pre-industrial period). The southern boundary of latitudinal permafrost is primarily determined by the zonal climate, by definition. Vandenberghe et al. (2012) demonstrated the sensitivity of permafrost boundaries to overlying climate impacted by sea-ice distribution. However, it is also highly dependent on other local modifying agents, such as snow, soil, vegetation, and topography. The subsurface physics and dynamics implemented in the current generations of the GCMs/ESMs may be very divergent in the way they handle these factors, as described by Koven et al. (2013), or in terms of total soil column depth (column 7 of Table 1). In fact, the formation, aggradation, maintenance, and degradation of permafrost are controlled not only by atmospheric temperature, but also by other factors such as wetness (precipitation, snow, soil moisture, drainage), soil (the composition of soil with matrix and organic materials, layering, and grain size distribution), vegetation, and micro-topography (aspect, face of slopes, roughness) (Shur and Jorgenson, 2007; Saito et al., 2013).

Due to this complexity of the subsystem, the subsurface isotherms do not necessarily coincide with the boundaries of permafrost zones, similar to the case of MAAT-permafrost zonation correspondence described in Introduction. Figure 5c compares distribution of the multi-model median of mean annual ground temperature (MAGT) for the permafrost regions for 0 k (red) and 21 k (blue). The 0 k MAGT distribution was compared to the observations obtained by a project "Permafrost Observatory Network: a Contribution to the Thermal State of Permafrost" (TSP) conducted during

CPD
9, 1565–1597, 2013

the International Polar Year (IPY; 2007–2009) in the Northern Hemisphere (IPY-TSP; Romanovsky et al., 2010, IPA, 2010). In Eurasia, there are areas of overestimation (cooling biases) between the −5 and −10 isotherms in eastern Siberia. In North America, to the contrary, southwestern part of Alaska showed underestimation (warm biases). These biases may relate to erroneous southward advance in eastern Siberia, and northward retreat in Alaska of the 0 k T_{sl}-based permafrost boundaries shown in Fig. 5a and b. Despite these regional discrepancies, overall correspondence between the modeled pre-industrial isotherms and the observations is surprisingly good, considering possible warming since the "pre-industrial" period (the mid-1800's), as argued in Sect. 4.1. In the Asian part of Russia, between 60° E and 120° E, the permafrost boundaries coincide well to the −5 °C isotherm, while in northern Canada the boundaries are slightly warmer; between 0 °C and −5 °C isotherms.

Similar to the LGM permafrost boundaries the LGM isotherms showed "latitudinal" characteristics in the middle of Eurasia. To its east, the orographic effects bent the isotherms to the south, while, to its west, the cooling influence of the ice sheet is apparent. Overall cooling of MAGT at the 21 k relative to the 0 k is about 5 °C both in Eurasia and Alaska.

The results in this study demonstrated that the direct and indirect methods can be used in combination compensating mutually. Reconstruction of frozen ground distribution using the GCMs/ESMs can be done through three approaches: statistical, physical offline (standalone), and physical online (coupled) approaches. The T_{as}-based method is a statistical approach, while the T_{sl}-based is a physical coupled one. These three approaches all have advantages and disadvantages, but maybe not mutually exclusive. Simplicity and ease in computation and application (in terms of time, space, and coding) are advantages of the statistical method; however it may lack physical justification when the assumptions or background conditions upon which the relationships were built have changed. In contrast, GCMs/ESMs can compute the subsurface temperature and other variables directly in a physically consistent way. Disadvantages of this method include high load of the computational resources, and general inflexibility

CPD
9, 1565–1597, 2013

to change the experimental settings (for example, spatial resolutions, choice of processes to be included in the experiments). Multi-layered, or multi-tiered use of those approaches, including offline (one-way) simulations using the physical subsurface models (e.g., Fig. 4 of Saito et al., 2013, by Marchenko and Romanovsky with their spatially distributed permafrost model GIPL-1.3l), will aid us more effectively to widen and deepen our understanding on the role and contributions of frozen ground subsystem, and impact of its change in the global eco-climate system.

6 Conclusions and implications

Frozen ground distribution at LGM was reconstructed from the multi-experiment analysis using the multi-model ensembles from PMIP2 and PMIP3 GCM simulations. Direct (soil temperature based) and indirect (surface air temperature based) estimation approaches were employed, and both showed results more consistent for the present-day and glacial periods, in comparison with previously known distributions compiled in multiple observational studies. The PMIP3 soil temperature output from the models with finer horizontal resolutions and improved model climatology produced a refined reconstruction with regional details and quantitative information on the subsurface thermal regime for the LGM period. Both the direct and indirect approaches proved to be successful in many aspects, each showing different strength and shortcomings, which prove somewhat mutually complementary.

Larger inter-model diversity of soil temperature based distribution has implied that the subsurface regime is still at the development phase, and suggests the substantial possibility of improvement, in terms of both resolved processes (parameterizations) and specification of subsurface characteristics (e.g., total soil column depth, thickness of soil layers, choice of appropriate physical property values). Coupling, such as between thermal and hydrological processes (including snow dynamics) and with biogeochemical processes, is definitely a necessary step in the next generation. Interactions and feedback with vegetation and ecological processes are very important

CPD
9, 1565–1597, 2013

to understanding the stability and variability of the Arctic terrestrial subsystem in the changing global eco-climate system. To this end, transitional integration, across the late Pleistocene though the Holocene deglaciation to the present-day, with differing complexity of implemented mechanisms and resolutions, will provide multi-tiered information regarding different aspects of the frozen ground subsystem in the past and present climate system, and its future projections.

Supplementary material related to this article is available online at: http://www.clim-past-discuss.net/9/1565/2013/cpd-9-1565-2013-supplement.pdf.

Acknowledgements. This study was supported by the National Science Foundation of the US under ARC-0327664. Portions of this research were conducted under the JAMSTEC-IARC Collaboration Study, with funding provided by the Japan Agency for Marine-Earth Science and Technology (JAMSTEC) under a grant to the International Arctic Research Center (IARC). This paper is also partly supported by the GRENE Arctic Climate Change Research Project. The authors acknowledge the World Climate Research Programme's Working Group on Coupled Modelling, which is responsible for CMIP, and we thank the climate modeling groups listed in Table 1 of this paper for producing and making available their model output. For CMIP, the US Department of Energy's Program for Climate Model Diagnosis and Intercomparison provides coordinating support and has led development of software infrastructure in partnership with the Global Organization for Earth System Science Portals. The authors also acknowledge the international modeling groups for providing their data for analysis, and the Laboratoire des Sciences du Climat et de l'Environnement (LSCE) for collecting and archiving model data. The PMIP2/MOTIF Data Archive is supported by CEA, CNRS, the EU project MOTIF (EVK2-CT-2002-00153) and the Programme National d'Etude de la Dynamique du Climat (PNEDC). The analyses here were performed using version 5 September 2008 of the database. More information is available at http://pmip2.lsce.ipsl.fr/ and http://motif.lsce.ipsl.fr/. The authors thank Nate Bauer (International Arctic Research Center, University of Alaska Fairbanks) for language proofreading and editing of the manuscript.

CPD
9, 1565–1597, 2013

References

Alexeev, V. A., Nicolsky, D. J., Romanovsky, V. E., and Lawrence, D. M.: An evaluation of deep soil configurations in the CLM3 for improved representation of permafrost, Geophys. Res. Lett., 34, L09502, doi:10.1029/2007GL029536, 2007.

Anisimov, O. A. and Nelson, F. E.: Permafrost Zonation and climate change in the Northern Hemisphere: Results from transient general circulation models, Climate Change, 35, 241–258, 1997.

Argus, D. F. and Peltier, W. R.: Constraining models of postglacial rebound using space geodesy: A detailed assessment of model ICE-5G (VM2) and its relatives, Geophys. J. Int., 181, 697–723, doi:10.1111/j.1365-246X.2010.04562.x, 2010.

Baulin, V. V. and Danilova, N. S.: Dynamics of Late Quaternary permafrost in Siberia, in: Late Quaternary environments of the Soviet Union, edited by: Velichko, A. A., University of Minesota Press, Minneapolis, 69–78, 1984.

Baulin, V. V., Danilova, N. S., Nechayev, V. P., Péwé, T. L., and Velichko, A. A.: Permafrost: Maximum cooling of the Last Glaciation (about 20,000 to 18,000 yrB.P.), in: Atlas of Paleoclimates and Paleoenvironments of the Northern Hemisphere, edited by: Frenzel, B., Pécsi, M., and Velichko, A. A., Geographical Research Institute, Hungarian Academy of Sciences, Budapest, Gustav Fischer Verlag, Stuttgart, p. 49, 1992.

Boeckli, L., Brenning, A., Gruber, S., and Noetzli, J.: A statistical approach to modelling permafrost distribution in the European Alps or similar mountain ranges, The Cryosphere, 6, 125–140, doi:10.5194/tc-6-125-2012, 2012a.

Boeckli, L., Brenning, A., Gruber, S., and Noetzli, J.: Permafrost distribution in the European Alps: calculation and evaluation of an index map and summary statistics, The Cryosphere, 6, 807–820, doi:10.5194/tc-6-807-2012, 2012b.

Braconnot, P., Otto-Bliesner, B., Harrison, S., Joussaume, S., Peterchmitt, J.-Y., Abe-Ouchi, A., Crucifix, M., Driesschaert, E., Fichefet, Th., Hewitt, C. D., Kageyama, M., Kitoh, A., Laîné, A., Loutre, M.-F., Marti, O., Merkel, U., Ramstein, G., Valdes, P., Weber, S. L., Yu, Y., and Zhao, Y.: Results of PMIP2 coupled simulations of the Mid-Holocene and Last Glacial Maximum – Part 1: experiments and large-scale features, Clim. Past, 3, 261–277, doi:10.5194/cp-3-261-2007, 2007.

CPD
9, 1565–1597, 2013

Brown, J., Ferrians Jr., O. J., Heginbottom, J. A., and Melnikov, E. S.: Circum-arctic map of permafrost and ground ice conditions. Boulder, CO: National Snow and Ice Data Center, Digital media, revised 2001, 1998.

Christiansen, H. H., Etzelmüller, B., Isaksen, K., Juliussen, H., Farbrot, H., Humlum, O., Johansson, M., Ingeman-Nielsen, T., Kristensen, L., Hjort, J., Holmlund, P., Sannel, A. B. K., Sigsgaard, C., Åkerman, H. J., Foged, N., Blikra, L. H., Pernosky, M. A., and Ødegård, R.: The thermal state of permafrost in the Nordic areaduring IPY 2007–2009, Permafrost Periglac., 21, 156–181, 2010.

Delisle, G.: Numerical simulation of permafrost growth and decay, J. Quat. Sci., 13, 325–333, 1998.

Delisle, G., Caspers, G., and Freund, H.: Permafrost in north-central Europe during the Weichselian: how deep?, in: Proceedings of 8th International Conference on Permafrost, Zurich, Switzerland, Belkama Publishers: Lisse; 187–191, 2003.

Frauenfeld, O. W., Zhang, T., Barry, R. G., and Gilichinsky, D.: Interdecadal changes in seasonal freeze and thaw depths in Russia, J. Geophys. Res., 109, D05101, doi:10.1029/2003JD004245, 2004.

Frauenfeld, O. W., Zhang, T., and McCreight, J. L.: Northern hemisphere freezing/thawing index variations over the twentieth century, Int. J. Climatol., 27, 47–63, 2007.

French, H. M.: The periglacial environment, 3rd Edn., Wiley, Chichester, 2007.

Frenzel, B., Pécsi, M., and Velichko, A. A. (Eds.): Atlas of Paleoclimates and Paleoenvironments of the Northern Hemisphere, Geographical Research Institute, Hungarian Academy of Sciences, Budapest, 153 pp., Gustav Fischer Verlag, Stuttgart, 1992.

Gates, W. L.: The Numerical Simulation of Ice-Age Climate with a Global General Circulation Model, J. Atmos., Sci., 33, 1844–1873, 1976.

Gruber, S.: Derivation and analysis of a high-resolution estimate of global permafrost zonation, The Cryosphere, 6, 221–233, doi:10.5194/tc-6-221-2012, 2012.

Harris, S. A.: Climatic Relationships of permafrost zones in areas of low winter snow-cover, Arctic, 34, 64–70, 1981.

Harris, S. A.: Identification of permafrost zones using selected permafrost landforms. Climate and Permafrost, 4th Canadian Permafrost Conference, 49–58, 1982.

Hubberten, H. W., Andreev, A., Astakhov, V. I., Demidov, I., Dowdeswell, J. A., Henriksen, M., Hjort, C., Houmark-Nielsen, M., Jakobsson, M., Kuzmina, S., Larsen, E., Pekka Lunkka, J., Lysså, A., Mangerud, J., Möller, P., Saarnisto, M., Schirrmeister, L., Sher, A. V., Siegert,

CPD
9, 1565–1597, 2013

C., Siegert, M. J., and Svendsen, J. I.: The periglacial climate andenvironment in northern Eurasia during the Last Glaciation, Quaternary Sci. Rev., 23, 1333–1357, 2004.
International Permafrost Association (IPA): IPA-IPY Thermal State of Permafrost (TSP) Snapshot Borehole Inventory, Version 1.0. Version 1 [indicate subset used], Boulder, Colorado USA: National Snow and Ice Data Center, 2010.
Kitover, D. C., Renssen, H., Van Balen, R. T., and Vandenberghe, J.: Modeling Permafrost Response of the Last Glacial Termination: First Results of the VAMPER Model, in: Tenth International Conference on Permafrost, 1, edited by: Hinkel, K. H., The Northern Publisher, Salekhard, 209–214, 2012.
Koven, C., Riley, W., and Stern, A.: Analysis of permafrost thermal dynamics and response to climate change in the CMIP5 Earth System Models, J. Climate, online first, doi:10.1175/JCLI-D-12-00228.1, 2012.
Lachenbruch, A. H., Sass, J. H., Marshall, B. V., and Moses Jr., T. H.: Permafrost, Heat Flow, and the Geothermal Regime at Prudhoe Bay, Alaska, J. Geophys. Res., 87, 9301–9316, 1982.
Lambeck, K., Purcell, A., Zhao, J., and Svensson, N.-O.: The Scandinavian Ice Sheet: from MIS 4 to the end of the Last Glacial Maximum, Boreas, 39, 410–435, doi:10.1111/j.1502-3885.2010.00140.x, 2010.
Lawrence, D. M. and Slater, A. G.: A projection of severe near-surface permafrost degradation during the 21st century, Geophys. Res. Lett., 32, L24401, doi:10.1029/2005GL025080, 2005.
Lawrence, D. M. and Slater, A. G.: The contribution of snow condition trends to future ground climate, Clim. Dynam., 34, 969–981, 2010.
Matsuoka, N.: Climate and material controls on periglacial soil processes: Toward improving periglacial climate indicators, Quaternary Res., 75, 356–365, 2011.
Mitchell, T. D. and Jones, P. D.: An improved method of constructing a database of monthly climate observations and associated high-resolution grids, Int. J. Climatol., 25, 693–712, 2005.
Nelson, F. E.: (Un)frozen in time, Science, 299, 1673–1675, 2003.
Nicolsky, D. J., Romanovsky, V. E., Alexeev, V. A., and Lawrence, D. M.: Improved modeling of permafrost dynamics in a GCM land-surface scheme, Geophys. Res. Lett., 34, L08501, doi:10.1029/2007GL029525, 2007.

CPD
9, 1565–1597, 2013

Ono, Y.: The Northern Landbridge of Japan, Quaternary Res. (Daiyonki kenkyuu), 29, 183–192, 1990.
Ono, Y.: Glacial and periglacial paleoenvironments in the Japanese Islands, Quaternary Res. (Daiyonki kenkyuu), 30, 203–211, 1991.
Osterkamp, T. E. and Gosink, J. P.: Variations in Permafrost Thickness in Response to Changes in Paleoclimate, J. Geophys. Res., 96, 4423–4434, 1991.
Petit-Maire, N., Bouysse, P., de Beaulieu, J.-L., Boulton, G., Guo, Z., Iriondo, M., Kershaw, P., Lisitsyna, O., Partridge, T., Pflaumann, U., Schulz, H., Soons, J., Van Vliet-Lanoë, B., Yuan, B., and van der Zijp, M.: Geological records of the recent past, a key to the near future world environments, Episodes, 23, 230–246, 2000.
Ramstein, G., Kageyama, M., Guiot, J., Wu, H., Hély, C., Krinner, G., and Brewer, S.: How cold was Europe at the Last Glacial Maximum? A synthesis of the progress achieved since the first PMIP model-data comparison, Clim. Past, 3, 331–339, doi:10.5194/cp-3-331-2007, 2007.
Romanovsky, V. E., Drozdov, D. S., Oberman, N. G., Malkova, G. V., Kholodov, A. L., Marchenko, S. S. , Moskalenko, N. G., Sergeev, D. O., Ukraintseva, N. G., Abramov, A. A., Gilichinsky, D. A., and Vasiliev, A. A.: Thermal State of Permafrost in Russia, Permafrost Periglac., 21, 136–155, 2010a.
Romanovsky, V. E, Smith, S. L., and Christiansen, H. H.: Permafrost Thermal State in the Polar Northern Hemisphere during the International Polar Year 2007–2009: a Synthesis, Permafrost Periglac., 21, 106–116, 2010b.
Rozenbaum, G. E. and Shpolyanskaya, N. A.: Late Cenozoic Permafrost History of the Russian Arctic, Permafrost Periglac., 9, 247–273, 1998.
Saito, K.: Arctic Land Hydro-thermal Sensitivity under Warming: Idealized Off-Line Evaluation of Physical Terrestrial Scheme in Global Climate Model, J. Geophys. Res.-Atmos., 113, D21106, doi:10.1029/2008JD009880, 2008.
Saito, K.: Paleo-permafrost distribution downscaled in South America and Northeastern Asia: Comparison of the GCM-based maps with the observations, in: Tenth International Conference on Permafrost, 4, The Northern Publisher, Salekhard, 490–491, 2012.
Saito, K., Kimoto, M., Zhang, T., Takata, K., and Emori, S.: Evaluating a high-resolution climate model: Simulated hydrothermal regimes in frozen ground regions and their change under the global warming scenario, J. Geophys. Res.-Earth, 112, F02S11, doi:10.1029/2006JF000577, 2007.

CPD
9, 1565–1597, 2013

Saito, K., Marchenko, S., Romanovsky, V., Bigelow, N., Yoshikawa, K., and Walsh, J.: Thermally-Conditioned Paleo-permafrost Variations from Global Climate Modeling, SOLA, 5, 101–104, doi:10.2151/sola.2009-026, 2009.

Saito, K., Zhang, T., Yang, D., Marchenko, S., Barry, R. G., Romanovsky, V., and Hinzman, L.: Influence of the Physical Terrestrial Arctic in the Eco-climate System, Ecol. Appl., in press, 2013.

Shannon, C. E.: A mathematical theory of communication, AT & T. Tech. J., 27, 379–423 and 623–656, 1948.

Shur, Y. L. and Jorgenson, M. T.: Patterns of Permafrost Formation and Degradation in Relation to Climate and Ecosystems, Permafrost Periglac. , 18, 7–19, 2007.

Smith, S. L., Romanovsky, V. E., Lewkowicz, A. G., Burn, C. R., Allard, M., Clow, G. D., Yoshikawa, K., and Throop, J.: Thermal state of permafrost in North America: a contribution to the International Polar Year, Permafrost Periglac., 21, 117–135, doi:10.1002/ppp.690, 2010.

Sueyoshi, T. and Hamano, Y.: The variations of the permafrost thickness under the climate change after the Last Glacial Maximum, Extended Abstracts, 8th International Conference on Permafrost, 157–158, 2003.

Tarasov, L. and Peltier, W. R.: Greenland glacial history and local geodynamic consequences, Geophys. J. Int., 150, 198–229, doi:10.1046/j.1365-246X.2002.01702.x, 2002.

Tarasov, L. and Peltier, W. R.: Greenland glacial history, borehole constraints, and Eemian extent, J. Geophys. Res., 108, 2143, doi:10.1029/2001JB001731, 2003.

Taylor, K. E., Stouffer, R. J., and Meehl, G. A.: An Overview of CMIP5 and the experiment design, B. Am. Meteorol. Soc., 93, 485–498, doi:10.1175/BAMS-D-11-00094.1, 2012.

Trombotto, D.: Inventory of fossil cryogenic forms and structures in Patagonia and the mountains of Argentina beyond the Andes, S. Afr. J. Sci., 98, 171–180, 2002.

United Nation Environment Programm (UNEP): Policy Implications of Warming Permafrost, UNEP Report, available at: www.unep.org/pdf/permafrost.pdf (last access: 22 March 2013), 2012.

Vandenberghe, J., Cui, Z., Zhao, L., and Zhang, W.: Thermal-contraction-crack Networks as Evidence for Late-Pleistocene Permafrost in Inner Mongolia, China, Permafrost Periglac., 15, 21–29, 2004.

CPD
9, 1565–1597, 2013

Vandenberghe, J., Velichko, A., and Gorbunov, A.: Forcing factors of permafrost retreat: a comparison between LGM and present-day permafrost extent in Eurasia, edited by: Kane, D. L. and Hinkel, K. M., 9th Int. Conf. Permafrost Fairbanks, 29/7/8/2008, 327–328, 2008.

van Everdingen, R. (Ed.): Multi-language glossary of permafrost and related ground-ice terms, Boulder, CO: National Snow and Ice Data Center, revised May 2005, 1998.

Van Vliet-Lanoë, B.: Periglacial Geomorphology, in: Encyclopedia of paleoclimatology and ancient environments, edited by: Gornitz, V., Springer, Dordrecht, The Netherlands, 770–775, 2009.

Velichko, A. A. (Ed.): Late Quaternary environments of the Soviet Union, University of Minesota Press, Minneapolis, 1984.

Velichko, A. A. and Nechaev, V. P.: Cryogenic regions during the Last Glacial Maximum (permafrost), in: Atlas of Paleoclimates and Paleoenvironments of the Northern Hemisphere, Frenzel, B., Pécsi, M., and Velichko, A. A., Gustav Fischer Verlag, Stuttgart, 108–109, 1992.

Washburn, A. L.: Permafrost features as evidence of climatic change, Earth-Sci. Rev., 15, 327–402, 1980.

Xu, S., Xu, D., and Pan, B.: Outer limit of permafrost during the Last Glaciation in East China, in: Fifth International Conference on Permafrost, Tronheim, Norway, 1, 268–273, 1988.

Zhang, T., Frauenfeld, O. W., McCreight, J., and Barry, R. G.: Northern Hemisphere EASE-Grid annual freezing and thawing indices, 1901–2002, Boulder, CO: National Snow and Ice Data Center/World Data Center for Glaciology, Digital media, 2005.

CPD
9, 1565–1597, 2013

Table 1. Summary of model simulations in PMIP2 and PMIP3 used in the study. The horizontal resolution for land is given by number of grid boxes in the longitudinal and latitudinal directions. Number of soil layers are given for PMIP3 models, followed by the depth of the total soil column.

	PMIP2		PMIP3		Horizontal Resolution	Soil layers	
Model Name	0 k	21 k	0 k	21 k	(land)	(depth)	Modeling Center (or Group)
CCSM	x	x			128 × 64	–	National Center for Atmospheric Research
CNRM-CM33	x	x			128 × 64	–	Centre National de Recherches Météorologiques/Centre Européen de Rechercheet Formation Avancée en Calcul Scientifique
CSIRO-Mk3L	x				64 × 56	–	Commonwealth Scientific and Industrial Research Organization (CSIRO) and Bureau of Meteorology (BOM), Australia
ECHAM5-MPIOM1	x				96 × 48	–	Max-Planck-Institut für Meteorologie (Max Planck Institute for Meteorology)
HadCM3M2		x			96 × 73	–	Met Office Hadley Centre
IPSL-CM4-V1-MR		x			96 × 72	–	Institut Pierre-Simon Laplace
MIROC3.2-mocat, MIROC3.2.2-mocat	x	x			128 × 64	–	Center for Climate System Research (The University of Tokyo), National Institute for Environmental Studies, and Japan Agency for Marine-Earth Science and Technology
MRI-CGCM2.3.4fa, MRI-CGCM2.3.4nfa	x				128 × 64	–	Meteorological Research Institute
UBRIS-HadCM3M2	x				96 × 73	–	University of Bristol/Met Office Hadley Centre
CCSM4			x	x	288 × 192	15 (43.7 m)	National Center for Atmospheric Research
CNRM-CM5				x	256 × 128	–	Centre National de Recherches Météorologiques /Centre Européen de Recherche et Formation Avancée en Calcul Scientifique
GISS-E2-R				x	144 × 90	6 (3.5 m)	NASA Goddard Institute for Space Studies
IPSL-CM5A-LR			x	x	96 × 96	7 (7.0 m)	Institut Pierre-Simon Laplace
MIROC-ESM			x	x	128 × 64	6 (14.0 m)	Japan Agency for Marine-Earth Science and Technology, Atmosphere and Ocean Research Institute (The University of Tokyo), and National Institute for Environmental Studies
MPI-ESM-P			x	x	192 × 96	5 (9.6 m)	Max-Planck-Institut für Meteorologie (Max Planck Institute for Meteorology)
MRI-CGCM3			x	x	320 × 160	14 (10.0 m)	Meteorological Research Institute

CPD
9, 1565–1597, 2013

Table 2. Areas of frozen ground in million km^2 simulated by the models in PMIP2 and PMIP3 for the preindustrial and LGM period, and the difference between the two era. PF3 denotes T_{sl}-based diagnosis in PMIP3. FG3 and FG2 denote T_{as}-based diagnosis in PMIP3 and PMIP2, respectively. Values are given in median, followed by the minimum and maximum (left and right numbers in the square parenthesis, respectively). At the bottom, numbers of models used for deriving the statistics for each category are given.

[million km^2]		21 k	0 k	Δ (21 k–0 k)
Continuous permafrost zone	PF3	25.6 [20.5, 26.4]	12.7 [11.1, 19.3]	12.9
	FG3	21.7 [16.8, 31.8]	11.8 [8.9, 12.9]	9.9
	FG2	15.7 [14.7, 20.7]	13.6 [9.7, 19.9]	2.1
Discontinuous permafrost zone	PF3	2.0 [0.1, 8.1]	1.6 [0.0, 11.1]	0.4
	FG3	4.4 [3.6, 6.6]	6.7 [4.6, 8.0]	−2.3
	FG2	4.5 [3.8, 5.1]	6.4 [5.4, 9.2]	−1.9
Seasonally freezing zone	PF3	22.5 [16.4, 28.3]	32.6 [20.7, 44.2]	−10.1
	FG3	23.9 [17.6, 27.9]	34.7 [32.9, 37.3]	−10.8
	FG2	23.4 [19.1, 27.4]	34.4 [31.3, 41.8]	−10.0
# of models	PF3	6	5	
	FG3	7	5	
	FG2	7	5	

CPD
9, 1565–1597, 2013

Table 3. Global areas (in million km^2) for maximum active layer thickness (ALT) and maximum seasonal freezing depth (SFD). Percentage for ALT relative to the total permafrost regions, and that of SFD relative to the total seasonally frozen ground regions are given in parentheses.

	ALT		SFD	
	LGM	piControl	LGM	piControl
0–1 m	8.4 (32.0 %)	1.3 (8.5 %)	8.4 (52.4 %)	20.3 (67.9 %)
1–2 m	12.9 (48.8 %)	9.7 (63.2 %)	5.0 (31.3 %)	7.6 (25.4 %)
> 2 m	5.1 (19.2 %)	4.3 (28.3 %)	2.6 (16.3 %)	2.0 (6.7 %)

CPD
9, 1565–1597, 2013

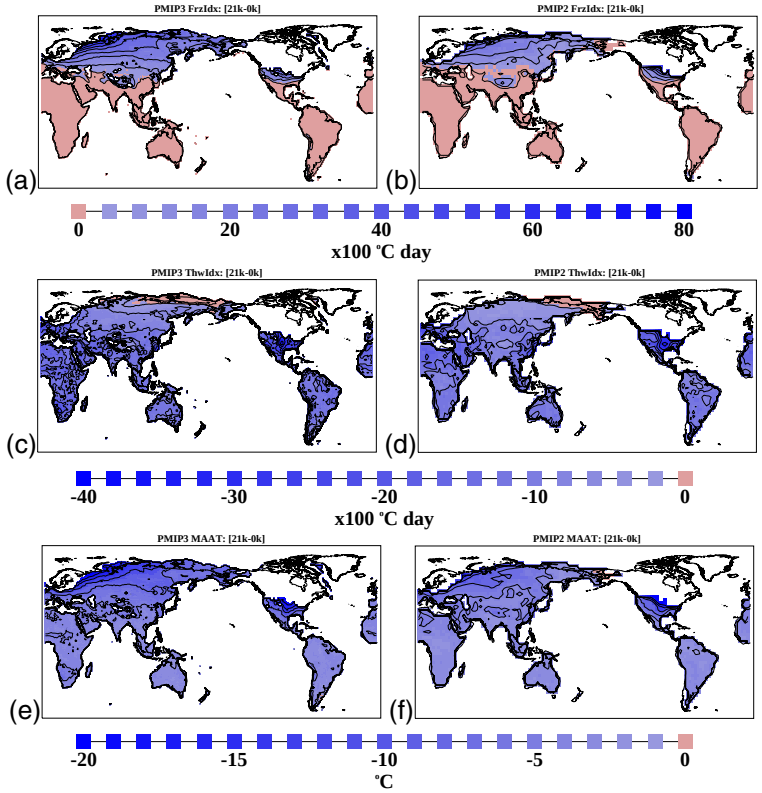

Fig. 1. Difference of the freeze index at the LGM period (21 k) from the pre-industrial (0 k), computed from **(a)** the PMIP3 simulations and **(b)** PMIP2. **(c)** and **(d)** Same as **(a)** and **(b)** except for the freeze index. **(e)** and **(f)** Same as **(a)** and **(b)** except for the mean annual air temperature at the surface (MAAT).

CPD
9, 1565–1597, 2013

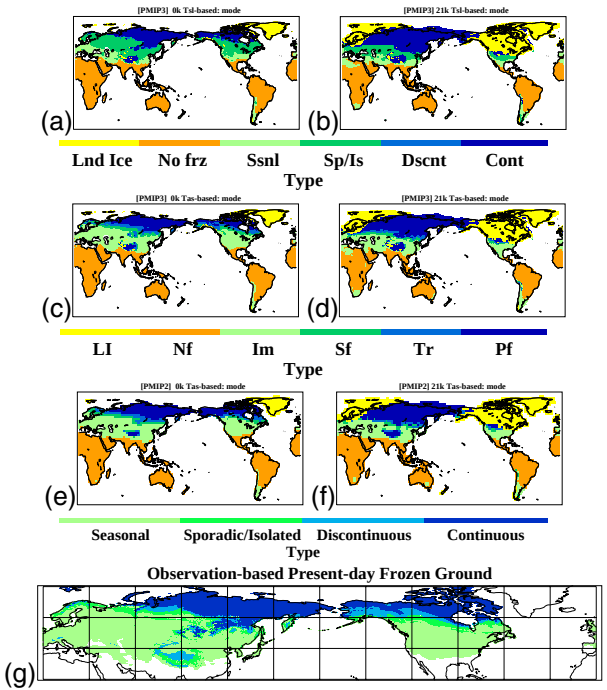

Fig. 2. Frozen ground distribution diagnosed from the T_{sl} for **(a)** the preindustrial and **(b)** the LGM periods by the PMIP3 results. Multi-model mode (the most frequent categories in each grid box) was used. Colors denote permafrost zone (Pf; dark blue), transitional zone (Tr; blue), seasonally freezing zone (Sf; dark green), intermittently freezing zone (If; pale green), no freezing zone (Nf; orange), and ice sheets (LI; yellow). **(c)** and **(d)** Same as **(a)** and **(b)** except that the diagnosis are T_{as}-based. **(e)** and **(f)** Same as **(c)** and **(d)** except for the PMIP2 results. **(g)** Observation-based frozen ground distribution at the present-day. Permafrost distribution was taken from the IPA map (Brown et al., 1997) and the seasonally freezing ground is determined by the mean monthly air temperature at the surface (Saito et al., 2007).

CPD
9, 1565–1597, 2013

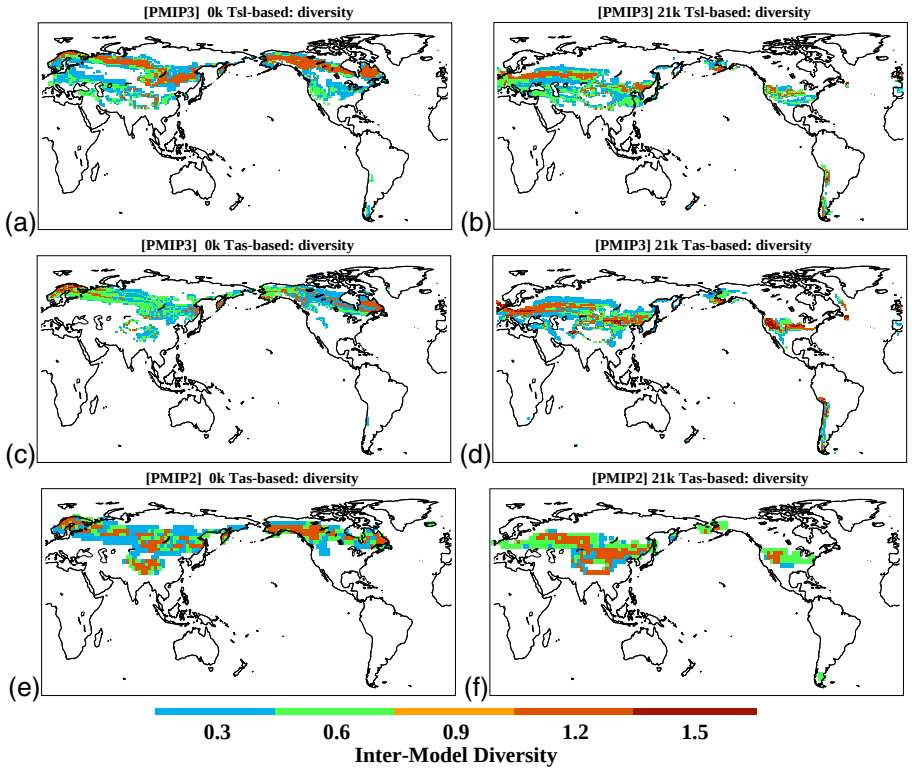

Fig. 3. (a) to **(f)** Same as Fig. 2 except for the inter-model diversity of the diagnosed frozen ground categories. For definition of the diversity index see text.

CPD
9, 1565–1597, 2013

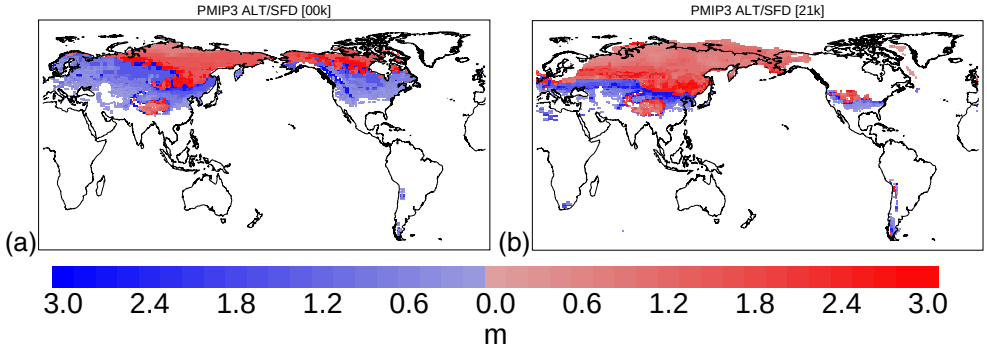

Fig. 4. (a) Multi-model median of maximum active layer depth (in red; for permafrost zones) and seasonal freezing depth (in blue; for seasonally frozen ground zones) for the pre-industrial period. **(b)** Same as **(a)** except for the LGM period.

CPD
9, 1565–1597, 2013

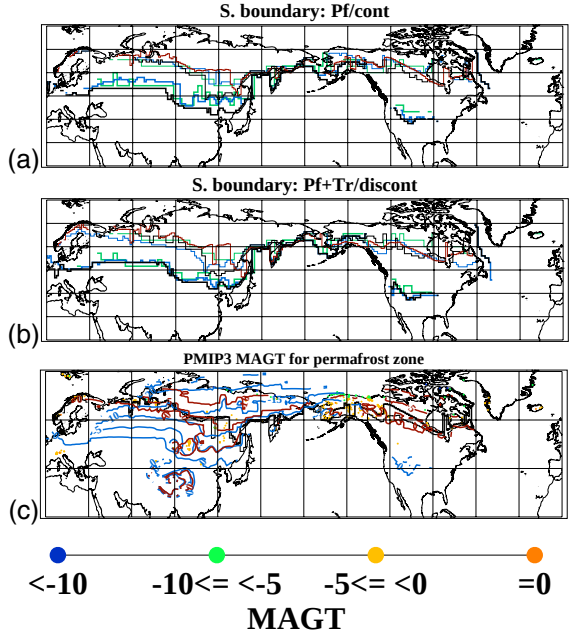

Fig. 5. Southern boundary of the latitudinal permafrost zones in the Northern Hemisphere for **(a)** continuous and **(b)** discontinuous permafrost for the pre-industrial (thin lines) and LGM (thick lines) period as defined in Fig. 2a and b, respectively. The boundaries for the T_{sl}-based diagnosis are shown in black while those for the T_{as}-based diagnosis are shown in blue for PMIP3 and green for PMIP2. Observed boundaries for the present-day are shown by red line. **(c)** Multi-model median of mean annual ground temperature (MAGT) for the pre-industrial (red) and LGM (blue) period. Contour interval is 5 °C. Only temperatures below 0 °C on the exposed land areas are shown. The observed boundaries for the present-day are reproduced from **(a)** and **(b)** in black thick and thin lines, respectively. Observed MAGT by IPY-TSP are shown by closed circles.

CPD
9, 1565–1597, 2013